Strain induced electronic structure changes in magnetic transition metal oxides thin films

G. van der Laan,[1] R. V. Chopdekar,[2] Y. Suzuki,[2] and E. Arenholz[3]

[1]*Diamond Light Source, Chilton, Didcot, Oxfordshire OX11 0DE, United Kingdom*
[2]*Department of Materials Science and Engineering, UC Berkeley, Berkeley, CA 94720*
[3]*Advanced Light Source, Lawrence Berkeley National Laboratory, Berkeley, CA 94720*

(Dated: June 22, 2010)

We show that the angular dependence of x-ray magnetic circular dichroism (XMCD) is strongly sensitive to strain induced electronic structure changes in magnetic transition metal oxides. We observe a pronounced dependence of the XMCD spectral shape on the experimental geometry as well as non-vanishing XMCD with distinct spectral features in transverse geometry in compressively strained $MnCr_2O_4$ films. The XMCD can be described as a linear combination of an isotropic and an angular dependent anisotropic contribution, the latter linearly proportional to the axial distortion due to strain. The XMCD spectra are well reproduced by atomic multiplet calculations.

PACS numbers: 68.60.Bs, 78.70.Dm, 78.20.Bh, 75.50.Gg

The delicate balance between charge, spin, orbital, and lattice degrees of freedom in transition metal oxides leads to unique phenomena such as colossal magnetoresistance [1], high temperature superconductivity, [2] as well as a remarkable diversity of charge, spin, and orbital ordered phases. The rich phase diagrams are determined by the strong local interaction of electrons in transition metal d orbitals [3]. Subtle changes in d occupancy and overlap—and thereby phase transitions—can be induced by variations in temperature, by external fields, through doping, and lattice distortions. Especially the strong coupling of the electronic properties with structural parameters allows controlling the physical characteristics of nanoarchitectures through strain at interfaces of layered and nanocomposite heterostructures [4–8]. Here we show that the angular dependence of the x-ray magnetic circular dichroism (XMCD) signal provides unique insights into the impact of strain on the electronic structure of magnetic transition metal oxides.

For an isotropic system, magnetically saturated by an external field, the XMCD signal scales with the angle, θ, between the field and x-ray beam as $\cos\theta$. [9] Consequently, in transverse geometry, i.e., perpendicular orientation of x rays and field ($\theta = 90°$), the XMCD signal vanishes completely. In systems with cubic magnetic anisotropy the XMCD spectrum is slightly different along $\langle 001\rangle$ and $\langle 111\rangle$ directions [10]. The angular dependence of the intensity of the XMCD spectral features can be well described by the lowest order term for the cubic anisotropy [10], however, the XMCD signal still disappears for $\theta = 90°$. This is no longer the case for systems with axial magnetic anisotropy, such as uniaxial, tetragonal, or trigonal symmetry of the lattice. In this case a non-vanishing integral of the XMCD signal indicates a non-zero component of the orbital magnetic moment perpendicular to the spin moment, a situation encountered in, e.g., thin films with strong uniaxial magnetic anisotropy. Whereas changes in the integrated intensity, proportional to the orbital moment, have been observed [11, 12], less attention has been paid to the detailed spectral shape of the XMCD and its correlation with structural distortions.

Here we determine the strain induced electronic structure changes in ferrimagnetic spinel $MnCr_2O_4$ films. The system does not exhibit any cubic magnetic anisotropy in slightly compressively strained films allowing us to unambiguously isolate the impact of an axial distorted cubic symmetry on the XMCD signal. We observe a pronounced angular dependence of the Mn^{2+} and Cr^{3+} $L_{3,2}$ XMCD as well as non-vanishing XMCD signals with distinct spectral features in transverse geometry. The experimental results are well reproduced using atomic multiplet calculations taking into account the reduced symmetry of the crystal lattice induced by the strain. This method holds promising perspectives for studying the electronic structure of magnetic oxide thin films.

$MnCr_2O_4$ epitaxial thin films were synthesized by pulsed laser deposition using stoichiometric single-phase targets at an energy density of 1-1.5 J/cm^2 on Nb-doped $SrTiO_3$(001) substrates held at 900 K. The samples were annealed in air for 9 h at 1100 K after deposition. While the theoretical lattice mismatch between $MnCr_2O_4$ and Nb-doped $SrTiO_3$ is 6.5%, x ray diffraction (XRD) measurements on the 55 nm thick $MnCr_2O_4$ films reveal a compressive strain of ∼0.9% indicating that the chosen film thickness and the post-growth annealing result in a partial relaxation of the strain. At a sample temperature of 20 K the Mn and Cr magnetic moments are collinear [13] and can be aligned in arbitrary directions by external fields below 0.5 T [see upper inset in Fig. 1(a)]. There is no indication of significant cubic magnetic anisotropy in the films. The XMCD signal was determined by independently varying the angle γ of the incident x-rays and angle μ of the magnetic field with respect to the sample normal using an eight-pole electromagnet [14]. The degree of circular polarization of the x-ray beam was 90%

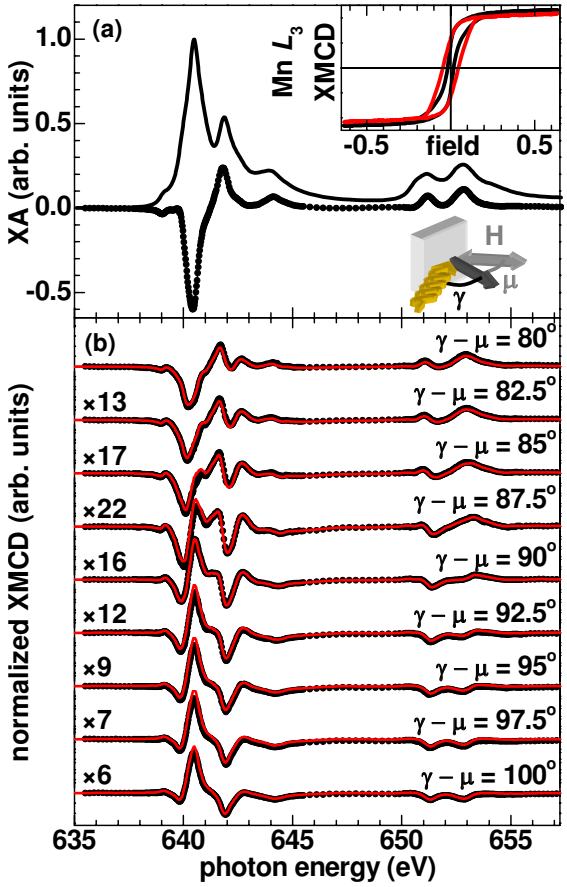

FIG. 1: (color online) (a) Mn $L_{3,2}$ XA spectrum (line) and XMCD signal (symbols) obtained from $MnCr_2O_4(001)$ at 20 K in external field **H** collinear with the x-ray beam impinging at an angle $\gamma = 54.7°$ relative to the surface normal. Upper inset shows Mn L_3 XMCD saturation loops: normal incidence (red) and at 30° grazing (black) with **H** ∥ **P** in both cases. Lower inset shows the experimental geometry. (b) Angular dependence of the XMCD for varying angle μ of the external field with $\gamma = 54.7°$. The XMCD signal is normalized to its most pronounced feature near 640 eV, where the scaling factor with respect to the XMCD for $\gamma - \mu = 0°$ is indicated for each spectrum. Lines (red) indicate the results of the model described in the text.

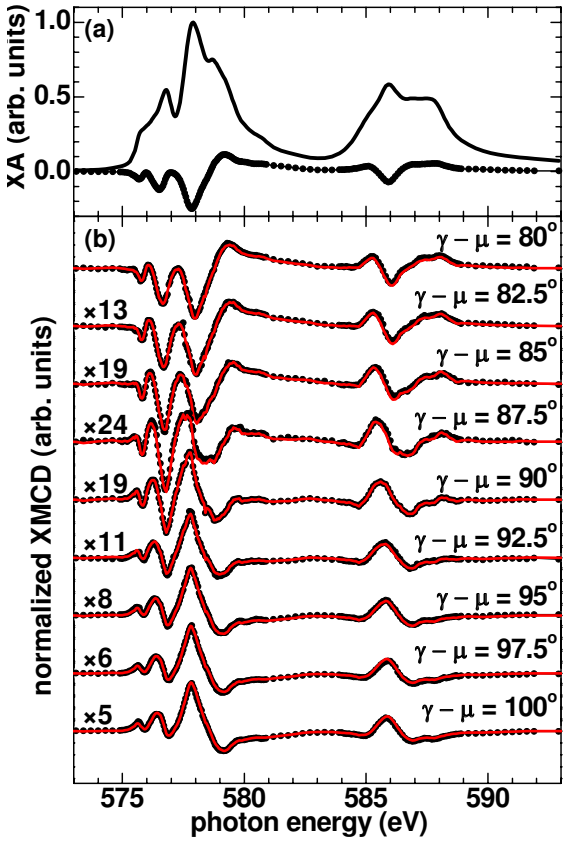

FIG. 2: (color online) (a) Cr $L_{3,2}$ XA spectrum (line) and XMCD signal (symbols) obtained from $MnCr_2O_4(001)$ at 20 K in external fields **H** collinear with the x-ray beam impinging at $\gamma = 54.7°$ relative to the surface normal. (b) Angular dependence of the XMCD for varying μ with $\gamma = 54.7°$. The XMCD signal is normalized to its most pronounced feature near 578 eV, with indicated scaling factor. Lines (red) indicate the results of the simulation described in the text.

for all measurements and the applied field 0.5 T. The XMCD spectra for $\gamma = \mu$ are the difference in x-ray absorption for parallel and antiparallel alignment of photon helicity and magnetic moments of Mn and Cr.

Figure 1(a) shows the Mn $L_{3,2}$ XA and XMCD for $\mu = \gamma = 54.7°$. The spectra agree with previous results for Mn^{2+} in tetrahedral (T_d) sites [10]. We determined the Mn $L_{3,2}$ XMCD angular dependence for $\gamma = 54.7°$ and varying μ near $\gamma - \mu = 90°$. To emphasize changes in spectral shape, the XMCD spectra normalized to their most pronounced feature near 640 eV are shown in Fig. 1(b) for $80° \leq \gamma - \mu \leq 100°$. It is evident that the XMCD shows pronounced changes in its spectral shape impacting the entire Mn $L_{3,2}$ spectral range. Variations in spectral shape are not restricted to the Mn $L_{3,2}$ XMCD. Figure 2(a) shows the Cr $L_{3,2}$ XA and XMCD spectra for $\mu = \gamma = 54.7°$ normalized to their most pronounced feature near 578 eV. The spectra agree with previous results for Cr^{3+} in octahedral (O_h) sites [15]. Figure 2(b) displays the Cr $L_{3,2}$ XMCD for varying angle of the Cr magnetic moments by ±10° to the sample normal.

The experimental results in Figs. 1(b) and 2(b) for both Mn and Cr indicate that the sign of the XMCD reverses for $\gamma - \mu$ sufficiently smaller and larger than 90°. Furthermore, the XMCD does not disappear at $\gamma - \mu = 90°$. In fact, the magnitude of the features is still considerable, i.e., 5-10% of that found for $\gamma = \mu$. We can exclude that the Mn and Cr XMCD for $\gamma - \mu = 90°$ is due to incomplete alignment of the Mn and Cr moments with the external field, in which case the XMCD spectral shape would be the same as for $\gamma = \mu$. As this is not the case there must be a different explanation for the non-vanishing XMCD signal with distinctly different spectral shape in transverse geometry.

The XMCD angular dependence can be described by

a linear combination of fundamental spectra accounting for the XA photon energy dependence in selected geometries with prefactors reflecting the symmetry of the experimental geometry. [16, 17] Since the photon helicity is a vector, there can be in arbitrary symmetry up to three different fundamental XMCD spectra. In orthorhombic lattice symmetry, for example, any XMCD spectrum can be written as linear combination of I_x, I_y, I_z, i.e. XMCD spectra obtained with x-rays and magnetization along $\hat{\mathbf{x}}$, $\hat{\mathbf{y}}$, and $\hat{\mathbf{z}}$, respectively:

$$I_{\rm XMCD} = I_x(\hat{\mathbf{P}}\cdot\hat{\mathbf{x}})(\hat{\mathbf{x}}\cdot\hat{\mathbf{M}}) + I_y(\hat{\mathbf{P}}\cdot\hat{\mathbf{y}})(\hat{\mathbf{y}}\cdot\hat{\mathbf{M}}) + I_z(\hat{\mathbf{P}}\cdot\hat{\mathbf{z}})(\hat{\mathbf{z}}\cdot\hat{\mathbf{M}}), \quad (1)$$

$\hat{\mathbf{P}}$ and $\hat{\mathbf{M}}$ are the x ray helicity vector and sample magnetization, respectively. This also means that each XMCD spectrum has a distinct angular dependence.

In axial symmetry, where $I_y = I_x$, there are only two different XMCD spectra. For small distortions I_x will be quite similar to I_z, so that it is beneficial to introduce the isotropic and quadrupolar or anisotropic XMCD spectrum, $I_0 = I_x + I_y + I_z$ and $I_2 = I_z - \frac{1}{2}(I_x + I_y)$, respectively, with very different shape and obviously $I_0 \gg I_2$. The angular dependent XMCD can be derived as [9]

$$\begin{aligned} I_{\rm XMCD} &= I_0\,\hat{\mathbf{P}}\cdot\hat{\mathbf{M}} + \frac{1}{2}I_2\left[3(\hat{\mathbf{P}}\cdot\hat{\mathbf{z}})(\hat{\mathbf{z}}\cdot\hat{\mathbf{M}}) - \hat{\mathbf{P}}\cdot\hat{\mathbf{M}}\right] \\ &= I_0\cos(\gamma-\mu) + \frac{1}{2}I_2\left[3\cos\gamma\cos\mu - \cos(\gamma-\mu)\right], \quad (2) \end{aligned}$$

where γ and μ are the angles of $\hat{\mathbf{P}}$ and $\hat{\mathbf{M}}$, respectively, with the $\hat{\mathbf{z}}$ axis of the axial symmetry, here the sample surface normal. Equation (2) shows that the pure I_0 and I_2 spectra are obtained in selected geometries. For $\gamma = \mu = 54.7°$, we obtain $I_{\rm XMCD} = I_0$. For $\gamma = 54.7°$ and $\gamma - \mu = 90°$, we find $I_{\rm XMCD} = I_2/\sqrt{2}$.

Using Eq. (2) we derived I_2 from the XMCD spectra measured for $\gamma - \mu = 90°$ and obtained I_0 from the XMCD signal observed for $\gamma - \mu = 70°$ employing the experimental I_2. The results are shown in Figs. 3 and 4. I_0 and I_2 exhibit distinctly different spectral features over the entire energy range of the Mn and Cr $L_{3,2}$ edges. For both metal sites, I_2 has ∼10% of the magnitude of I_0. We can model XMCD spectra for arbitrary geometries using the experimental spectra for I_0 and I_2 in Eq. (2) without free parameters. A comparison of the model with experimental data is shown in Figs. 1 and 2. The agreement is very good for both Mn and Cr. This confirms that for $MnCr_2O_4$ the angular dependence can be very well modeled taking into account only the axial distortion and neglecting the cubic magnetic anisotropy. An additional cubic magnetic anisotropy gives different XMCD spectra along 4-fold and 3-fold axes, [10] but there is no experimental evidence for such a contribution in $MnCr_2O_4$.

To obtain detailed information about electronic structure changes caused by strain induced lattice distortions, we performed atomic multiplet calculations [18, 19]. For a system with axially distorted cubic symmetry the

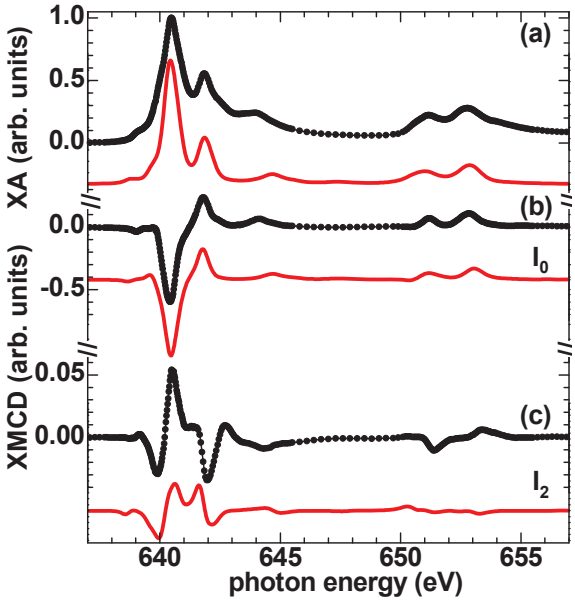

FIG. 3: (color online) Comparison of experimental (solid symbols, black) and theoretical (lines, red) data with $Dq = -0.05$ and $Cp = 0.006$ eV for the Mn $L_{3,2}$ edges in $MnCr_2O_4$. (a) XA spectrum, (b) isotropic XMCD spectrum, I_0, and (c) quadrupolar XMCD spectrum, I_2.

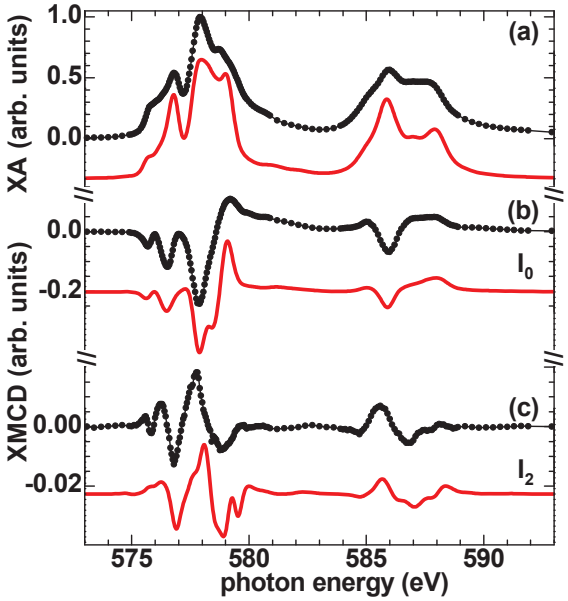

FIG. 4: (color online)Comparison of experimental (solid symbols, black) and theoretical (lines, red) data with $Dq = 0.2$ and $Cp = -0.006$ eV for the Cr $L_{3,2}$ edges in $MnCr_2O_4$. (a) XA spectrum, (b) isotropic XMCD spectrum, I_0, and (c) quadrupolar XMCD spectrum, I_2.

crystal-field operator is given as

$$V = D(x^4 + y^4 + z^4 - \frac{3}{5}r^4) + C(z^2 - \frac{1}{3}r^2), \quad (3)$$

where the first and second term describe the cubic and axial field, respecively. Combined with the radial part

TABLE I: One-electron representations and energies of d wave functions in a cubic electrostatic potential with axial distortion along C_4 axis. The energy contribution of the axial field, given in Eq. (3), is diagonal in the magnetic quantum number m and equal to $-2Cp\,[m^2 - \frac{1}{3}\ell(\ell+1)]$, where $\ell = 2$.

Representation	d-orbital	Wave function	Energy
b_1	$x^2 - y^2$	$\frac{1}{\sqrt{2}}[\|2\rangle + \|-2\rangle]$	$6Dq - 4Cp$
a_1	z^2	$\|0\rangle$	$6Dq + 4Cp$
b_2	xy	$\frac{1}{\sqrt{2}}[\|2\rangle - \|-2\rangle]$	$-4Dq - 4Cp$
e	xz, yz	$\|1\rangle, \|-1\rangle]$	$-4Dq + 2Cp$

of the d-wave function integrals, the parameters D and C supply the crystal-field parameters Dq and Cp for cubic and axial field [20]. Table I shows the one-electron energies of the d wave functions expressed in Dq and Cp.

The $L_{3,2}$ absorption spectra were calculated for electric-dipole allowed transitions $3d^n \rightarrow 2p^5 3d^{n+1}$ in the presence of the electrostatic field and a small magnetic exchange field of 0.01 eV. [21] Both the XA and I_0 spectra can be calculated, to good accuracy, in cubic symmetry, with the axial distortion introducing only a small change. Figures 3 and 4 show the comparison of experimental and calculated spectra for Mn^{2+} d^5 T_d ($Dq = -0.05$ eV) and Cr^{3+} d^3 O_h ($Dq = 0.2$ eV), indicating a very good agreement. To calculate I_2, it is necessary to include the axial distortion because this spectrum otherwise vanishes. For modest values of Cp, compared to the cubic parameter Dq, the magnitude of I_2 scales linearly with Cp. This provides unique means to determine the parameter value by comparison to the experiment. We obtain best agreement with the ratio $I_2/I_0 \approx 0.1$ for $Cp = +0.006$ eV and -0.006 eV for Mn and Cr, respectively [22]. Table I shows that for Cr O_h with positive Dq and negative Cp the d_{xy} state has the lowest energy while for Mn T_d with negative Dq and positive Cp the $d_{x^2-y^2}$ state has the lowest energy. This means that for both metal sites the electrostatic potential is higher along z, which implies a compressive strain. This is in agreement with our XRD results of 0.9% compressive strain in $MnCr_2O_4$ film by the Nb-doped $SrTiO_3$ substrate. There is in fact another easy way to derive the size and direction of the strain. Using Eq. (2) it can be shown that for compressive (tensile) strain the I_{XMCD} in Figs. 1 and 2 obtains a minimum for $\alpha \equiv \gamma - \mu - 90^\circ$ is negative (positive), where α scales with the size of the strain. In our case, $\alpha \approx -2.5^\circ$, in agreement with the compressive strain.

It is of great practical interest that a very small axial distortion ($Cp/Dq \ll 1$) already gives a dramatic effect in the angular dependence of the XMCD, easily discernible in transverse geometry. This opens the opportunity to study strain in magnetic transition metal oxide using soft x ray spectroscopy and microscopy techniques on ultrafast time scales with nanometer spatial resolution in element, valence, and site specific way. The angular dependent XMCD is a general phenomenon that will occur in anisotropic systems, such as metal sites at surfaces, interfaces, and biological systems. Decomposition of the XMCD into different spectra, each with its unique angular dependence makes it possible to detect even small anisotropies. In the case of $MnCr_2O_4$, both the specific angular dependence and the spectral shape give strong support to the model that the XMCD signal is sensitive to the axial distortion along a four-fold axis in cubic symmetry.

Supported by the U.S. Department of Energy under Contract No. DE-AC02-05CH11231.

[1] S. Jin, T. H. Tiefel, M. McCormack, R. A. Fastnacht, R. Ramesh, and L. H. Chen, Science **264**, 413 (1994).

[2] J. G. Bednorz and K. A. Muller, Z. Phys. B **64**, 189 (1986).

[3] M. Imada, A. Fujimori, and Y. Tokura, Rev. Mod. Phys. **70**, 1039 (1998).

[4] F. Tsui, M. C. Smoak, T. K. Nath, and C. B. Eom, Appl. Phys. Lett. **76**, 2421 (2000).

[5] I. Bozovic, G. Logvenov, I. Belca, B. Narimbetov, and I. Sveklo, Phys. Rev. Lett. **89**, 107001 (2002).

[6] J. Wang, J. B. Neaton, H. Zheng, V. Nagarajan, S. B. Ogale, B. Liu, D. Viehland, V. Vaithyanathan, D. Schlom, U. V. Waghmare, et al., Science **299**, 1719 (2003).

[7] J. H. Haeni, P. Irvin, W. Chang, R. Uecker, P. Reiche, Y. L. Li, S. Choudhury, S. Choudhury, W. Tian, M. Hawley, et al., Nature **430**, 758 (2004).

[8] J. L. MacManus-Driscoll, P. Zerrer, H. Wang, H. Yang, J. Yoon, A. Fouchet, R. Yu, M. G. Blamire, and Q. X. Jia, Nature Mat. **7**, 314 (2008).

[9] G. van der Laan, Phys. Rev. B **57**, 5250 (1998).

[10] K. W. Edmonds, G. van der Laan, A. A. Freeman, N. R. S. Farley, T. K. Johal, R. P. Campion, C. T. Foxon, B. L. Gallagher, and E. Arenholz, Phys. Rev. Lett. **96**, 117207 (2006).

[11] H. A. Dürr and G. van der Laan, Phys. Rev. B **54**, R760 (1996).

[12] H. A. Dürr, G. van der Laan, and B. T. Thole, Phys. Rev. Lett. **76**, 3464 (1996).

[13] K. Tomiyasu, J. Fukunaga, and H. Suzuki, Phys. Rev. B **70**, 214434 (2004).

[14] E. Arenholz and S. O. Prestemon, Rev. Sci. Instrum. **76**, 083908 (2005).

[15] N. D. Telling, V. S. Coker, R. S. Cutting, G. van der Laan, C. I. Pearce, R. A. D. Pattrick, E. Arenholz, and J. R. Lloyd, Appl. Phys. Lett. **95**, 163701 (2009).

[16] G. van der Laan, J. Phys. Soc. Jpn. **63**, 2393 (1994).

[17] G. van der Laan, Lect. Notes Phys. **697**, 143 (2006).

[18] G. van der Laan and B. T. Thole, Phys. Rev. B **43**, 13401 (1991).

[19] G. van der Laan and I. W. Kirkman, J. Phys.: Condens. Matter **4**, 4189 (1992).

[20] B. N. Figgis, J. Chem. Soc. p. 4887 (1965).

[21] Ground and final state wave functions were calculated at $T = 0$ in intermediate coupling using Cowan's code with relativistic correction. The atomic Hartree-Fock values of the Slater and spin-orbit parameters are tabulated in Ref.

[19]. Interatomic screening and mixing was taken into account by scaling the Slater integrals by a factor 0.7 for Cr d^3 and 0.91 for Mn d^5. The calculated results were broadened by a Lorentzian of $\Gamma = 0.1$ (0.35) eV for the L_3 (L_2) edge to account for intrinsic linewidth broadening and a Gaussian of $\sigma = 0.15$ eV for instrumental broadening.

[22] The cubic plus axial field is equivalent to a tetragonal field of D_{4h} symmetry of the same Dq value, with $Dt = 0$ and $Ds = -2Cp$. We therefore also performed calculations in D_{4h} with $Dt \neq 0$, which leads to a small additional XMCD contribution.